Check for updates

Efficient removal of bisphenol pollutants on imine-based covalent organic frameworks: adsorption behavior and mechanism†

Daijun Fu,[a] Qianxin Zhang,[b] Ping Chen,[a] Xiaoshan Zheng,[a] Jun Hao,[a] Peiying Mo,[a] Haijin Liu,[c] Guoguang Liu [ID][a] and Wenying Lv [ID]*[a]

The extensive use of bisphenol analogues in industry has aggravated the contamination of the water environment, and how to effectively remove them has become a research hotspot. This study presents two imine-based covalent organic frameworks with different pore sizes (COFs) [TAPB (1,3,5-tris(4-aminophenyl)benzene)-Dva (2,5-divinylterephthaldehyde)-PDA (terephthalaldehyde) (COF-1), and TAPB (1,3,5-tris(4-aminophenyl)benzene)-Dva (2,5-divinylterephthaldehyde)-BPDA (biphenyl dialdehyde) (COF-2)], which have achieved the efficient adsorption of bisphenol S (BPS) and bisphenol A (BPA). The maximum adsorption capacity of COF-2 for BPS and BPA obtained from Langmuir isotherms were calculated as 200.00 mg g^{-1} and 149.25 mg g^{-1}. Both hydrogen bonding and π–π interactions might have been responsible for the adsorption of BPS and BPA on the COFs, where the high adsorption capacity of COFs was due to their unique pore dimensions and structures. Different types of pharmaceutical adsorption studies indicated that COF-2 exhibited a higher adsorption performance for different types of pharmaceuticals than COF-1, and the adsorption capacity was ranked as follows: bisphenol pharmaceuticals > anti-inflammatory pharmaceuticals > sulfa pharmaceuticals. These results confirmed that COFs with larger pore sizes were more conducive to the adsorption of pollutants with smaller molecular dimensions. Moreover, COF-1 and COF-2 possessed excellent pH stability and recyclability, which suggested strong potential applications for these novel adsorbents in the remediation of organic pollutants in natural waterways and aqueous ecosystems.

1. Introduction

In recent years, myriad synthetic organic chemicals such as pharmaceuticals, personal care products, and endocrine disruptors have been extensively used and subsequently discharged into various aquatic environments, which has raised widespread concern regarding the safety of the water environment.[1] Bisphenol A (BPA) and bisphenol S (BPS), as representative bisphenol contaminants, have been frequently detected in ambient waterways, which increased their long-term potential toxicity risks to aquatic ecosystems and humans.[2,3] Previous reports have confirmed that the main hazards of bisphenol analogues were related to biological toxicity and endocrine disrupting effects.[4] With growing global concerns

and increasingly stringent legal requirements related to the emission of synthetic organic chemicals, it is urgent to investigate simple and effective strategies for the removal of bisphenol contaminants from aqueous environments.

To date, various techniques have been explored for the removal of bisphenols contaminants from aqueous environments, including adsorption,[5] chemical precipitation,[6] biological degradation[7] and photocatalytic degradation.[8] Compared with other methods, adsorption was regarded as an important method in basic research and industrial applications in terms of its operational simplicity and low cost.[9] Adsorbent is considered to be the most important part of the adsorption process, which determines the adsorption performance and economic benefits. Many traditional adsorption materials such as activated carbon (AC),[10] carbon nanotubes (CNTs),[11] zeolites,[12] graphene oxide (GO)[13] and metal–organic frameworks (MOFs),[14] were used to eliminate the pollution of bisphenols contaminants. An ideal adsorbate usually needs to include three aspects: (i) excellent adsorption capacity and fast adsorption rate; (ii) great regeneration performance; (iii) the preparation process is simply and environmentally friendly. Unfortunately, the existing adsorbents cannot meet the above three conditions at the same time. Thus, it is necessary to

[a]School of Environmental Science and Engineering, Guangdong University of Technology, Guangzhou, 510006, China. E-mail: lvwy612@163.com; Fax: +86-13538982812; Tel: +86-20-39322547

[b]School of Environmental, State Key Joint Laboratory of Environmental Simulation and Pollution Control (SKLESPC), Beijing Key Laboratory for Emerging Organic Contaminants Control, Tsinghua University, Bejing, 100084, China

[c]Key Laboratory for Yellow River and Huaihe River Water Environment and Pollution Control, School of Environment, Henan Normal University, Xinxiang 453007, China

develop novel adsorbents that combines the above three aspects to remove bisphenol pollutants in the water environment.

Covalent organic frameworks (COFs) is an emerging class of crystalline porous organic polymers, with low densities, extensive surface areas, adjustable pore sizes, and excellent chemical and thermal stability.[15] Owing to these remarkable properties, COFs have emerged as a novel porous adsorbent with strong prospects in broad applications for the resolution of currently serious energy and environmental related challenges, including gas adsorption,[16] optoelectronics,[17] catalysis,[18] proton conduction,[19] and much more. Recently, COFs demonstrated excellent adsorption performance for the removal of pharmaceuticals and personal care products (DCF, BPA, SMT, *etc.*),[20–23] heavy metal ions (Pb^{2+}, Cu^{2+}, Cr^{6+}, *etc.*),[24–27] and dyes (methyl blue, rhodamine B, methyl orange, *etc.*) from water solutions.[28,29]

Although the adsorption performance of COFs for the target pollutants have been explored, the adsorption characteristics and mechanism, particularly the molecular-scale mechanisms involved in pollutant adsorption processes, have not been comprehensively elucidated. Therefore, it is necessary to deeply study the interaction mechanism between COFs and target pollutants. Additionally, previous research verified that imine COFs with good water stability and abundant C=N binding sites were a good choice for the removal of the contaminant from wastewater, COFs with different pore sizes can be prepared through skeleton design to remove pollutants of specific molecular sizes. Thus, we explored and studied the behavior and mechanism of imine-based COFs on bisphenols pollutants in wastewater, and confirming the structure and physical–chemical properties by a vary of characterization. Adsorption experiments were performed to verify the adsorption performance of the prepared COF.

In this work, we systematically investigated the adsorption behaviors and mechanisms of two imine-based COFs (COF-1 and COF-2) for the treatment of two bisphenol analogues (BPS and BPA). The main contents of this work were as follows: (i) the preparation and characterization of COFs; (ii) the adsorption performance of the COFs for the removal of BPS and BPA under different parameters (*e.g.*, contact time, concentration, temperature, pH, and ionic strength). (iii) The adsorption mechanisms of the COFs for BPS and BPA were revealed *via* pH and XPS analysis; (iv) different types of pharmaceuticals adsorption study (*e.g.*, nonsteroidal anti-inflammatory pharmaceuticals and sulfa pharmaceuticals) were employed to further confirm the adsorption mechanisms.

2. Materials and methods

2.1. Chemicals and materials

All the chemicals were purchased from commercial suppliers and used without further purification. 1,3,5-Tris(4-aminophenyl) benzene (TAPB, purity 98%), 2,5-divinylterephthaldehyde (Dva, purity 98%), terephthalaldehyde (PDA, purity 98%), and biphenyl dialdehyde (BPDA, purity 98%) were obtained from Shanghai Kaiyulin Biological Technology Co. Ltd. (Shanghai, China). 1,3,5-Trimethylbenzene (AR, 97%) (mesitylene), 1-butanol (*n*-BuOH) (AR, 99%), methanol (AR, 99%), acetone (AR, 99%), tetrahydrofuran (THF) (AR, 99%) and acetic acid (AcOH) (AR, 36%) were

purchased from Shanghai Aladdin Biochemical Technology Co. Ltd. (Shanghai, China). Drug adsorbates (purity 98%) including bisphenol S (BPS), bisphenol A (BPA), bisphenol B (BPB), bisphenol AF (BPAF), bisphenol F (BPF), diclofenac (DCF), and sulfamethoxazole (SMT) were obtained from Shanghai Maclin Biological Technology Co. Ltd. (Shanghai, China), which their physical–chemical properties are listed in Table 1.

2.2. Preparation of COFs

The COF-1 and COF-2 were synthesized *via* the methods of previous report with some slight modifications.[30] In a typical procedure of COF-1, a 25 ml schlenk tube was charged with TAPB (89.97 mg, 0.256 mmol), Dva (35.75 mg, 0.192 mmol), and PDA (25.75 mg, 0.192 mmol) in a solution of *n*-BuOH/mesitylene/3 M acetic acid (10 : 5 : 2 v/v/v, for a total of 6.8 ml). This mixture was sonicated for 5 min to form a homogeneous suspension. Subsequently, the tube was flash-frozen at liquid nitrogen temperature (77 K), evacuated, and sealed. Upon warming to room temperature, the tube was heated at 120 °C for three days under a static condition. After cooling, the yellow precipitate (COF-1) was isolated by centrifugation and rinsed with THF (3 × 15 ml) and ethanol (3 × 15 ml), and the material was dried overnight in a vacuum at 60 °C. The COF-2 was synthesized using a similar method but changing PDA to BPDA, and finally a yellow-brown powder was obtained.

2.3. Batch adsorption experiments

Batch adsorption experiments were performed to investigate the adsorption capacities of the prepared COFs. Typically, 8.0 mg of COFs powder was added to 40 ml bisphenol analogue solution with different initial concentrations, ranging from 10 to 80 mg L^{-1}, and the mixture oscillated for 24 h at 303 K, 220 rpm in a water bath constant temperature oscillator to attain equilibrium. Following adsorption, 1 ml suspension was extracted and filtered with a 0.45 μm filter membrane. The concentration of bisphenols was measured by high-performance liquid chromatography (HPLC), and the analysis of details can be found in Text S1.† The adsorption capacity (mg g^{-1}) of the COFs was calculated by the following equation:

$$q_e = \frac{(C_e - C_0) \times V}{m}$$

In which, C_0 (mg g^{-1}), and C_e (mg g^{-1}) are the initial concentration and that at the equilibrium (after 24 h), respectively, V (L) is the total volume of the bisphenol mixture, and m (g) is the mass of the adsorbent.
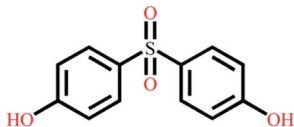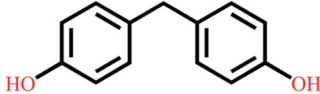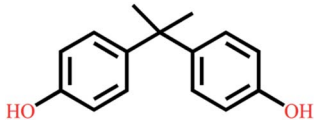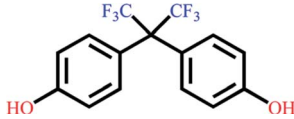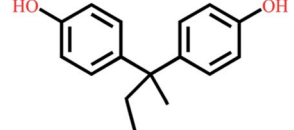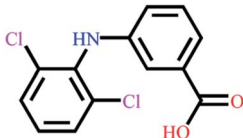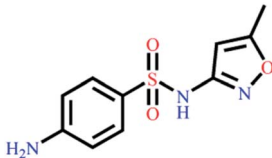
All experiments were performed in a 100 ml centrifuge tube protected from light to avoid the photodegradation of the BPS and BPA. The adsorption kinetics, adsorption equilibrium, adsorption thermodynamics, as well as the effect of pH and ionic strength, and the recyclability of the adsorbents were also investigated. All experiments were conducted in triplicate, with the experimental details described in Table 1.

2.4. Characterization of COFs

The surface morphology of the samples was observed using scanning electron microscopy (SEM, Hitachi SU-8220) and

Table 1 Structures and physicochemical properties of bisphenols pharmaceuticals, and other types of pharmaceuticals

Name	Chemicals formula	Molecular structure	Molecular weight	pK_{a1}/pK_{a2}	Log K_{ow}[a]	Molecular size [Å][b]
Bisphenol S	$C_{12}H_{10}O_4S$		250.27	7.42/8.03	1.65	4.23
Bisphenol F	$C_{13}H_{12}O_2$		200.23	9.84/10.45	3.06	4.15
Bisphenol A	$C_{15}H_{16}O_2$		228.29	9.78/10.39	3.32	4.36
Bisphenol AF	$C_{15}H_{16}F_6O_2$		336.23	9.13/9.74	4.47	4.67
Bisphenol B	$C_{16}H_{18}O_2$		242.31	9.77/10.38	4.13	4.49
Diclofenac	$C_{14}H_{11}Cl_2NO_2$		296.15	4.15	4.51	4.36
Sulfamethoxazole	$C_{10}H_{11}N3O_3S$		253.28	1.6/5.7	0.89	4.13

[a] Predicted data cited from http://chemspider.com, which are generated using the US Environmental Protection Agency's EPI Suite (KOWWIN v1.67). [b] The molecular size of pharmaceuticals were obtained from Material Studio 6.0.

transmission electron microscope (TEM, FEI Talos, F200S). X-ray diffraction (XRD) patterns were measured on a Bruker D8 Advance X-ray diffractometer (Bruker, Germany), where the 2 theta range of 0.5–40° and a scanning rate of 2° min^{-1}. Fourier transform infrared (FT-IR) spectroscopy was achieved by a spectrometer with a wave-number range 500–4000 cm^{-1}. A solid ^{13}C NMR experiment was recorded on an AVANCE III HD 400 Bruker Bio Spin Corp. A thermogravimetric instrument (TGA) was evaluated on a NETZSCH STA449F3 under N$_2$ conditions. The N$_2$ adsorption–desorption apparatus were conducted at 77 K with an ASAP 2020 instrument. All samples were degassed at 100 °C for 12 h before the actual measurements. The specific surface area and pore-size-distribution were obtained from the adsorption data using Langmuir and Brunauer–Emmett–Teller (BET) analysis and DFT methods, respectively. The point of zero charges (pH_{pzc}) was measured at varying pH values using the zeta potentials-pH curves with a 90 Plus particle size analyzer (Brookhaven, USA).

3. Results and discussion

3.1. Synthesis and characterization

As depicted in Scheme 1, TAPB was used as the knot, and Dva, PDA, BPDA as the linkers for the preparation of the COF-1 and COF-2. The condensation reactions were performed under solvothermal reactions by using n-butanol and mesitylene as solvents and 3 M acetic acid as catalyst at 120 °C for three days. COF-1 was a yellow powder with a 94% isolation yield. Simultaneously, COF-2 was prepared through a similar method except for changing PAD to BPAD, to finally obtain a yellow-brown powder with a 90% isolation yield.

The surface morphologies of the COF-1 and COF-2 were elucidated *via* scanning electron microscopy (SEM) and transmission electron microscopy (TEM) measurements. As shown in Fig. 1(a–d), the prepared COFs presented a non-uniform spherical morphology, in which the main spherical diameter of COF-1 was 1.6 nm and that of COF-2 was 2.5 nm. Compared
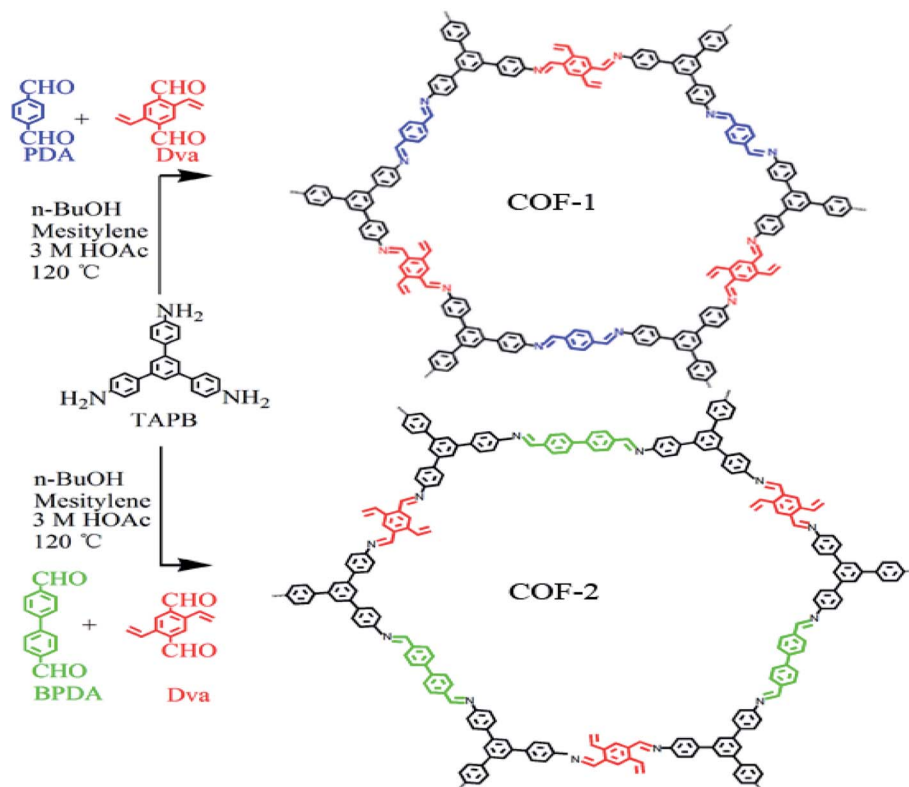
Scheme 1 The synthesis process of COF-1 and COF-2.

to COF-1, COF-2 exhibited a larger spherical size. This might be related to differences in the variety of reaction precursors and the quantity of acetic acid in the reaction system, which was consistent with previously reported results.[31] Furthermore, energy dispersion spectroscopy (EDS) mapping (Fig. 1(e–o)) confirmed the uniform distribution of C, N, and O element atoms in the entire COF samples.

The crystalline structures of COF-1 and COF-2 were revealed using Power X-ray diffraction (PXRD) measurements. As shown in Fig. 2(a), COF-2 displayed an intense peak at 2.7° that corresponded to the reflection from (100) facet, this confirmed the formation of crystalline structures. Meanwhile, the presence of broad peaks at 18.5° in COF-2 was attributed to the (001) facet, which indicated the periodicity and π–π stacking of the COF-2 layers.[32] Compared to COF-2, COF-1 also showed peaks at 2.9° and 18.8°, which were attributed to (100) and (001) facets, respectively. The relative weaken peaks in COF-2 indicated that COF-2 had lower crystallinity than COF-1.[33] The chemical stabilities of COF-1 and COF-2 were further investigated by PXRD after 24 h of treatment in a variety of solvents including water, HCl, NaOH, and MeOH. It was observed that the COFs were very stable in different solvents, as indicated by the almost unchanged PXRD patterns (Fig. S1(a and c)†). Additionally, the intensity of the PXRD pattern after adsorption decreased slightly, but the position of the characteristic peak did not change significantly, indicating that the structure of the COF material did not change (Fig. S1(b and d)†). These results confirmed that COFs displayed good chemical stability.

To verify the chemical structures and compositions of the COF-1 and COF-2, Fourier transform infrared (FT-IR) spectroscopy and solid-state ^{13}C NMR spectroscopy were performed. The FT-IR spectra (Fig. 2(b)) revealed that the complete disappearance of the characteristic N–H stretching vibration band (3340 cm^{-1}) and typical C=O stretching vibration band (1690 cm^{-1}) of the precursors, and the emerging peaks at 1600 cm^{-1} and 1605 cm^{-1} could be discovered in the FT-IR spectra of COF-1 and COF-2, respectively, which were attributed to the characteristic C=N stretching vibrations, indicating the successful polymerization between the monomers.[34,35] The carbon resonance observed by solid-state ^{13}C NMR (Fig. 2(c)) exhibited two typical signals for the –C=N– bonds at 157 ppm for the COF-1 and COF-2, respectively. The signal of the vinyl groups was observed at 115 ppm, whereas the signals from 127 ppm to 146 ppm were assigned to the carbons of the benzene ring building blocks, which further confirmed the formation of the COFs.[36] In addition, the thermal property of the COFs was also evaluated by TGA analysis. Two obvious weight-losses were observed in TGA curves. The first step occurred at 30 °C −100 °C was attributed to the water weight-losses. The second weight losses occurred at 400–580 °C mainly indicated the decomposition and combustion of the frameworks. It can be concluded that the thermal stability of COF-1 and COF-2 up to 400 °C (Fig. 2(d)).[37,38]

Nitrogen adsorption–desorption experiments were also conducted to estimate the porous properties of the COF-1 and COF-2. As presented in Fig. 2(e), the COF-1 and COF-2
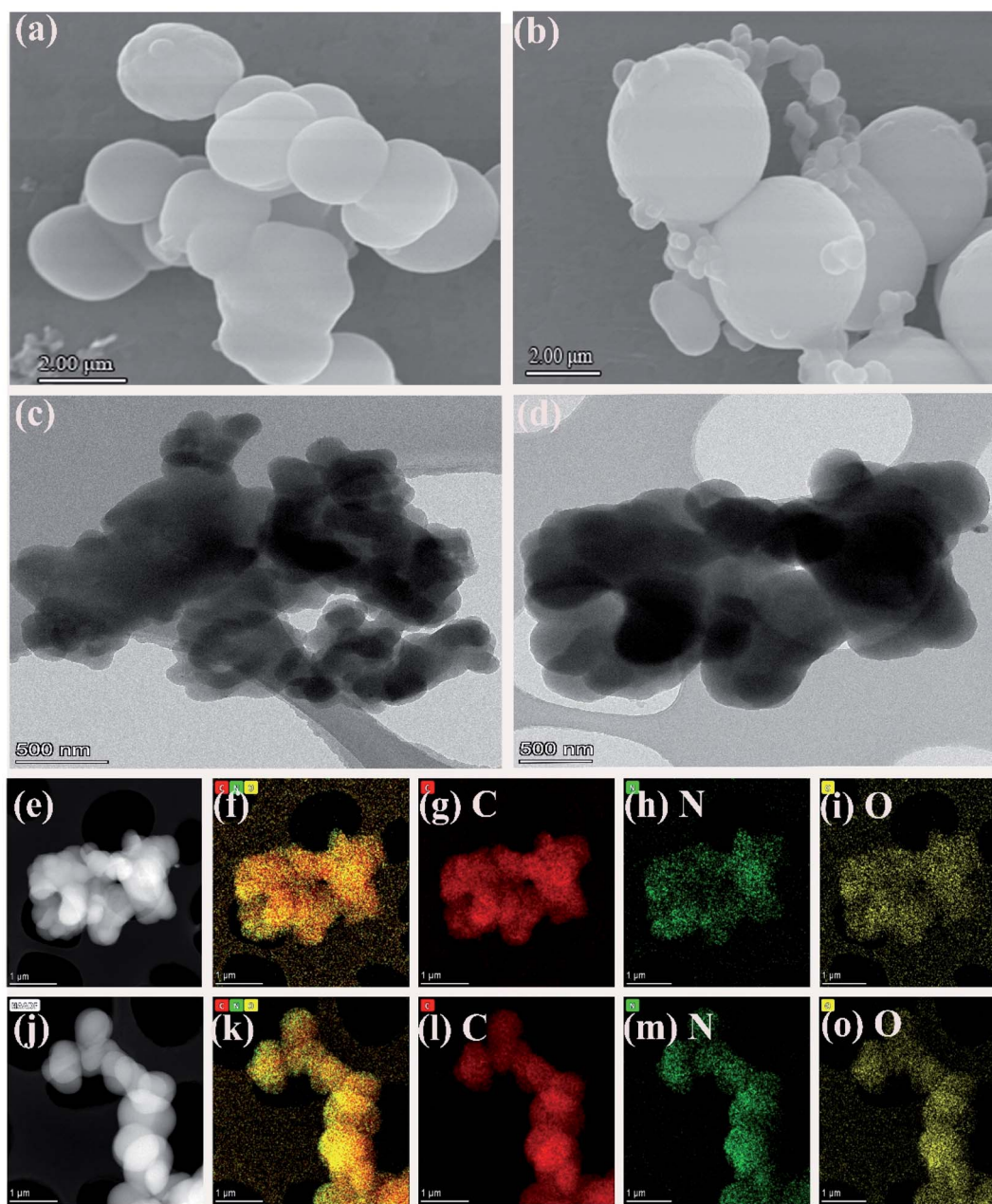
Fig. 1 (a and b) SEM images of COF-1 and COF-2; (c and d) TEM images of the COF-1 and COF-2; (e–i) mapping image of COF-1 containing C, N and O elements; (j–o) mapping image of COF-2 containing C, N and O elements.

adsorption curves exhibited nitrogen uptakes with a significant increase at low pressures ($P/P_0 = 0$–0.01), which indicated that the prepared COFs were porous materials. When using the Brunauer–Emmett–Teller (BET) model in the P/P_0 range between 0.05 and 0.25 (Fig. S2 and S3†), the BET areas of 190 m^2 g^{-1} for COF-1 and 51 m^2 g^{-1} for COF-2 could be obtained. According to a single point measurement ($P/P_0 = 0.99$), the total pore volumes of COF-1 and COF-2 were determined to be 0.12 cm^3 g^{-1} and 0.05 cm^3 g^{-1}, respectively. Furthermore, the pore size distribution of COF-1 and COF-2 were also evaluated by using the density functional theory (DFT). As illustrated in Fig. 3(d), inset, COF-1 and COF-2 showed a narrow pore size

distribution, with the main peaks at 1.59 nm and 2.51 nm, respectively. Moreover, the reasons for the narrow pore size distribution and the relatively low BET surface areas of COF-1 and COF-2 might likely be ascribed to the difficulty in the removal of residual solvents and guest molecules, which occupied the pore channels of the corresponding frameworks.[39,40]

3.2. Different types of pharmaceuticals adsorption study

The structural properties of COF-1 and COF-2 have been confirmed by various characterization techniques, which indicated the prepared materials were excellent adsorbents in
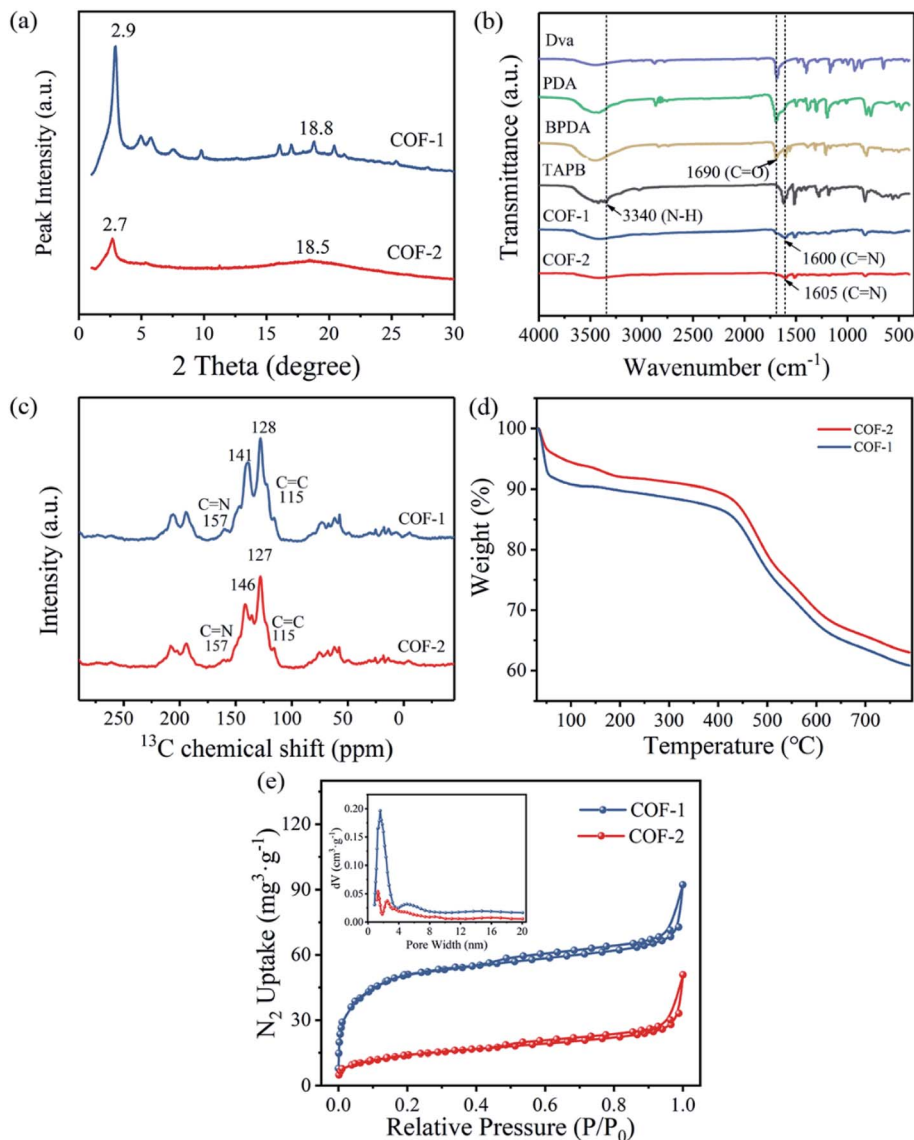
Fig. 2 (a) XRD patterns of COF-1and COF-2; (b) FT-IR spectrum of COF-1 and COF-2; (c) ^{13}C NMR spectra of COF-1 and COF-2; (d) TGA curves of COF-1 and COF-2; (e) N$_2$ adsorption–desorption isotherm, inset: pore-size distribution of COF-1 and COF-2.
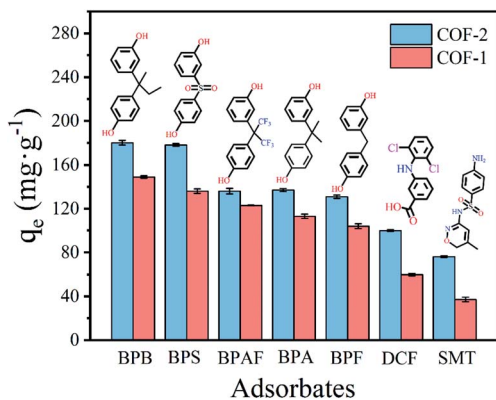

Fig. 3 Adsorption capacities of different types of pharmaceuticals onto COF-1 and COF-2 (in each case $C_0 = 50$ mg L^{-1}, $T = 303$ K, $t = 3$ h, $m/V = 0.2$ g L^{-1}).

theory. To verify this speculation, seven pollutants were utilized to investigate the adsorption performance of COFs absorbents, encompassing bisphenols pharmaceuticals (BPB, BPF, BPAF, BPS, BPA), nonsteroidal anti-inflammatory pharmaceuticals (DCF), and sulfa pharmaceuticals (SMT). The structures and physicochemical properties of seven pollutants were listed in Table 1. As depicted in Fig. 3, COFs showed relatively high performance in the adsorption of bisphenols pharmaceuticals with the removal capacity above 100 mg g^{-1}. The removal capacity of COF-1 and COF-2 to remove DCF was 59.82 mg g^{-1} and 99.98 mg g^{-1}, respectively. The absorbent's ability to eradicate sulfa pharmaceuticals was worst and could be ignored. Additionally, the performance of COF-2 was generally better than COF-1. The difference in adsorption might be related to the structure of pollutants. Bisphenol pharmaceuticals contained two polar functional groups (–OH*2), while DCF and SMT contained only one functional group, namely –COOH and

–NH$_2$, respectively. To explore a comprehensive view of the structure–activity relationship between structures of adsorbates and adsorption ability of COFs, we selected BPS and BPA as representative pollutants to conduct following adsorption experiments.

3.3. Adsorption performance

3.3.1. Adsorption kinetics. The adsorption kinetics were investigated to better understand the mechanisms of COFs for the adsorption of BPS and BPA. The effects of the contact time on the BPS and BPA by COF-1 and COF-2 were investigated and are shown in Fig. 4(a and b). COF-1 and COF-2 showed rapid adsorption rate for BPS and BPA in the first 0.5 h, and then the adsorption rate gradually decreased until reaching the adsorption equilibrium at 1 h. The fast adsorption for COF-1 and COF-2 could be attributed to the large pore size, specific adsorption sites and the abundant C=N functional groups, which could interact with pollutant molecular to form hydrogen-bonds and π–π interactions.[41]

To analyze the adsorption mechanism, the kinetics data were fitted by the pseudo-first-order model and pseudo-second-order kinetic model, and the kinetic parameters were listed in Table S1.† According to the fitted results, the values of the calculated adsorption amounts ($q_{e, cal}$) were closer to experimental values ($q_{e, exp}$) and the correlation coefficient R^2 values (>0.99) were much higher through the fitted pseudo-second-order, indicating that the adsorption process could be better fitted by the pseudo-second-order kinetics model. Furthermore, for the given adsorbent, higher k_2 values were achieved through the adsorption of BPS rather than BPA, which indicated a faster adsorption rate of BPS by COFs. The obvious difference in the adsorption rate may have been related to the sizes of the adsorbate molecules. As seen in Table 1, the molecular dimensions of the BPS (4.23 Å) and BPA (4.36 Å) were much smaller than the pore sizes of the prepared COF-1 (16 Å) and COF-2 (25 Å), which meant that they could easily pass through
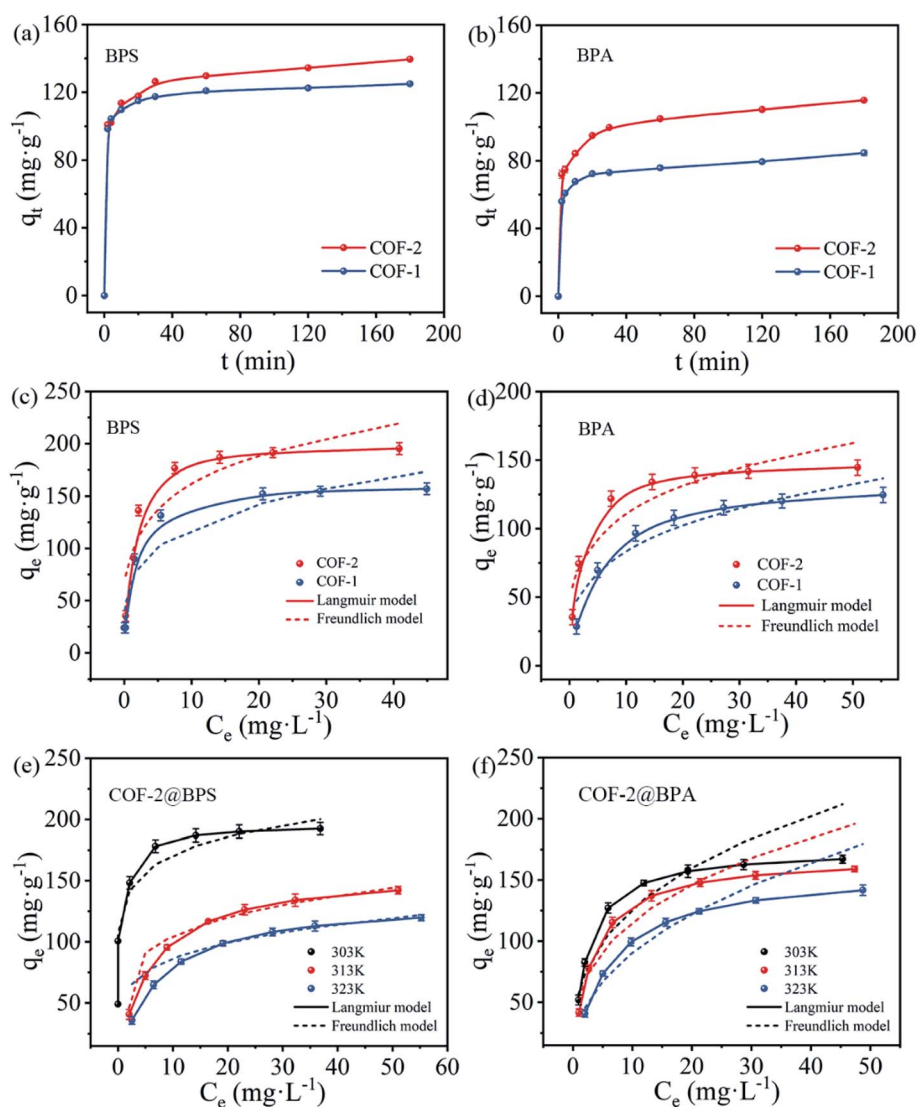

Fig. 4 (a and b) Adsorption kinetics of BPS and BPA onto COF-1 and COF-2 (C_0 = 30 mg L^{-1}, T = 303 K, t = 3 h, m/V = 0.2 g L^{-1}); (c and d) adsorption isotherm of BPS and BPA onto COF-1 and COF-2 at 303 K; (e and f) adsorption isotherms of BPS and BPA onto COF-2 at different temperatures (C_0 = 10–80 mg L^{-1}, T = 303–323 K, t = 24 h, m/V = 0.2 g L^{-1}).

the pores of the COFs.[42] Furthermore, the BPS had a smaller molecular size than BPA, which made the diffusion of BPS into the pores of the COFs easier, resulting in a faster adsorption rate. For the given adsorbate, COF-2 exhibited more rapid adsorption kinetics than COF-1, meaning that the larger pore size of COF-2 was more conducive to the diffusion of the pollutants molecular into the pores. Based on the above analysis, the importance of large COFs pore sizes for effective pollutant adsorption was demonstrated.

3.3.2. Adsorption isotherms and thermodynamics. The adsorption isotherm can reflect the interaction between the adsorbent and the adsorbate, while further explain the adsorption mechanism.[43] Fig. 4(c and d) showed the adsorption isotherms of COF-1 and COF-2 toward BPS and BPA at 303 K. It revealed that the adsorption capacities of both COF-1 and COF-2 increased with the increase of equilibrium concentration of BPS and BPA, then gradually attained adsorption saturation. It might have been due to the enhancement of the molecular driving force with the increased initial concentration, which accelerated the diffusion of BPS and BPA molecules into the channels of the COFs.

To elucidate the adsorption process, two isotherm models (Langmuir model and Freundlich model) were used to fit the resultant isotherms data, and the related parameters were listed in Table S2.† Compared with the Freundlich model, the Langmuir model was much better in describing the adsorption isotherms with a much higher correlation coefficient (R^2), which indicated that the adsorption process proceeded through monolayer adsorption.[44] The maximum adsorption capacities of COF-2 for BPS and BPA reached to 195 mg g^{-1} and 145 mg g^{-1}, respectively, which were much higher than COF-1 (157 mg g^{-1} for BPS and 125 mg g^{-1} for BPA). This result was consistent with the characterization analysis, which was ascribed to COF-2 with a larger pore size than COF-1. Moreover, BPS exhibited higher adsorption capacities than BPA, which may have been attributed to the disparate molecular structures and properties of these two chemicals. Notably, according to the Langmuir adsorption model, the adsorption capacities of COF-2 for BPS and BPA were 200.00 mg g^{-1} and 149.25 mg g^{-1}, respectively, which were higher than many other adsorbents reported previously (Table S3†).

Furthermore, the adsorption performance of COF-2 for BPS and BPA were also studied at different temperatures (303 K, 313 K, and 323 K) to evaluate the thermodynamic properties. Fig. 4(e and f) showed the thermodynamic isotherm, and the corresponding thermodynamics parameters were listed in Table S4.† The ΔG value continued to increase with rising temperature but remained negative, indicating that the adsorption process was spontaneous. However, higher temperatures weakened the spontaneity of the adsorption reaction, and it was averse to the adsorption of pollutants. Additionally, the negative values of ΔH demonstrated that the adsorption process was exothermic in nature, which was also confirmed by the decrease in the adsorption capacities of BPS and BPA with rising temperatures. The negative standard entropy change ΔS revealed that the randomness increased at the solid/liquid interface.[45]

3.3.3. Effect of solution pH and ionic strength. In consideration of practical applications, it was necessary to investigate the effects of the removal of organic pollutants under extreme

conditions, such as harsh pH values and high ionic strength. Fig. 5(a and b) showed the impacts of solution pH on the adsorption of BPS and BPA by COFs under an initial pH range of from 4.0 to 11.0. It can be seen that BPS and BPA demonstrated similar pH-dependent adsorption. Under acidic conditions (pH 4–7), COF-1 and COF-2 maintained a high adsorption performance for BPS and BPA, and the pH had no significant influence to the bisphenol containment capacity. Under alkaline conditions (pH 8–10), the adsorption capacities of COF-1 and COF-2 for BPS and BPA slightly decreased with higher OH$^-$ concentrations, where the downward trend of BPS was more obvious than that of BPA. In particular, when the pH value was increased to 11, the adsorption capacity dropped lower, which suggested that strong alkaline conditions were not conducive for the adsorption of bisphenols.

The above phenomena have been explained by the electrostatic interactions between the adsorbate species and the charge states of the adsorbents under different pH values.[46] Fig. 5(c) showed that the zero-point potential (pH_{pzc}) was 4.3 for COF-1 and 7.2 for COF-2. At the tested pH conditions (8–11), the adsorbents were negatively charged, and their negative charges increased with rising pH. Meanwhile, BPS and BPA might also be deprotonated under higher pH values. Under these conditions, it was difficult for negatively charges BPS/BPA to be adsorbed on the surfaces of negatively charged COFs. Electrostatic repulsion likely accounted for the decreasing adsorption capacity at high pH values.[47] However, electrostatic interactions cannot completely explain the BPS/BPA adsorption onto COFs under the acidic conditions, as BPS/BPA was in their molecular form, thus, the electrostatic attraction would not occur between the COFs and bisphenols. Consequently, there must have been extra interactions occurring between the COFs and bisphenols pollutants, that enabled the COFs to maintain high adsorption capacities under a broad pH range.

It was well acknowledged that ambient water bodies contain not only various organic pollutants, but also contain high concentrations of salts, which might influence the removal of contaminants. Thus, a study was also performed on the effects of the ion strength on the adsorption of BPS and BPA by COFs. Fig. 5(d and e) showed the adsorption of BPS and BPA on COF-1 and COF-2 under different concentration of NaCl. As NaCl concentration increased, the adsorption affinities have not changed significantly. Several studies showed that increase ionic strength can affect the adsorption of organic pollutants to some extent due to the salting-out effect or electrostatic screening effect.[48,49] Other researchers found that salt addition have a squeezing-out effect on the adsorbent, which was unfavorable for the adsorption of pollutants.[50] Thence, the effect of ionic strength on adsorption depended on the relative contribution of these two effects. In the present study, the ionic strength has negligible effect on the adsorption of BPS and BPA by COFs, indicating the two opposite effects were equivalent or too weak. Additionally, the adsorption of BPS/BPA on COFs was driven by hydrogen-bonding and π–π interactions (see detailed discussion below). These factors could not be significantly modified by changing the ionic strength in a small range.
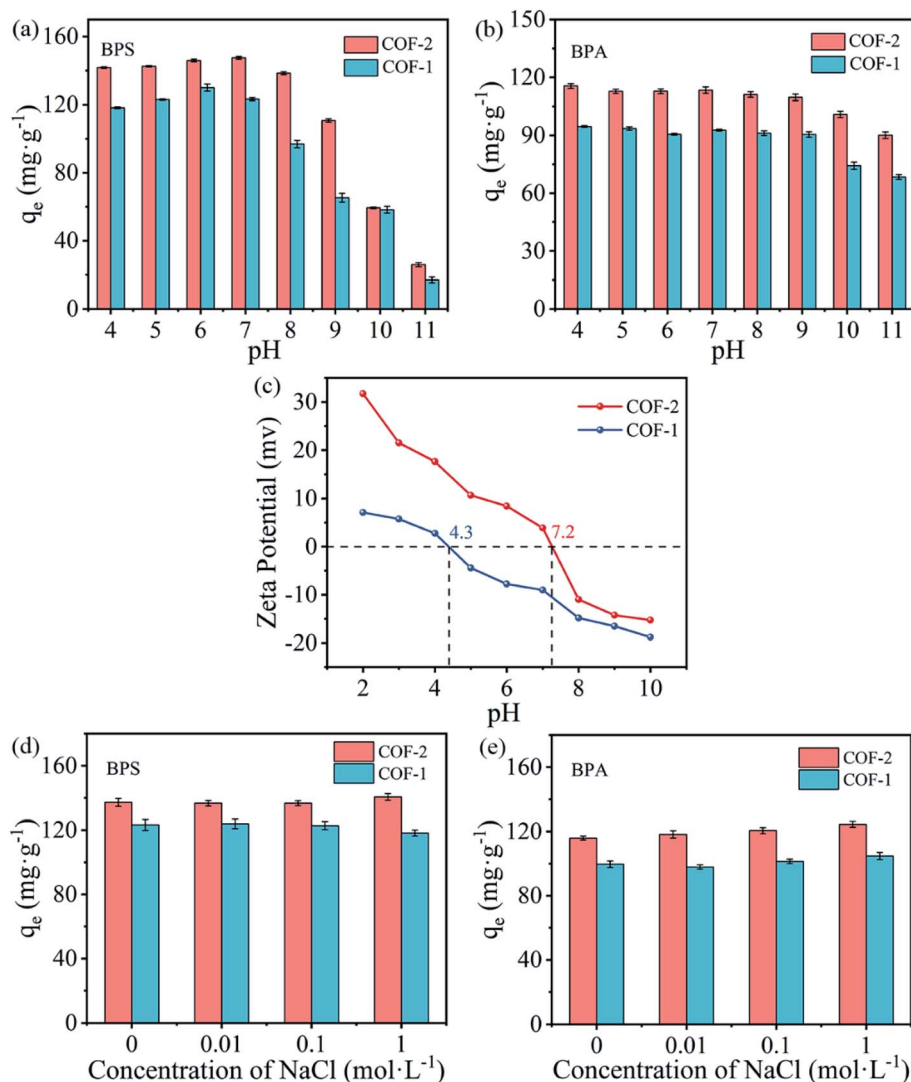
Fig. 5 (a and b) Effect of pH on BPS and BPA adsorption onto COF-1 and COF-2; (pH = 4–11, C_0 = 30 mg L^{-1}, T = 303 K, t = 3 h, m/V = 0.2 g L^{-1}); (c) zeta potential of COF-1 and COF-2; (d and e) the effect of ions strength on BPS and BPA adsorption onto COF-1 and COF-2 (NaCl concentration = 0–1 mol L^{-1}, C_0 = 30 mg L^{-1}, T = 303 K, t = 3 h, m/V = 0.2 g L^{-1}).

3.4. Adsorption mechanism

Generally, the adsorption capacity of adsorbents increased with the enlargement of the specific surface area when there was no distinct adsorption site.[51] However, compared with the specific surface area of COF-1 (190 m^2 g^{-1}), COF-2 with a smaller specific surface area (51 m^2 g^{-1}) was more effective for the removal of BPS and BPA. This indicated that surface area was not the main factor that affected the adsorption, and there was a specific interactive mechanism between the adsorbent and adsorbates. According to the previous report, the adsorption performance of organic pollutants on porous materials was not only affected by intrinsic characteristics (*e.g.*, charge, size and electronic states), but also by the weak intermolecular interactions (*e.g.*, hydrogen-bonding and π–π interactions), hydrophobic interactions, electrostatic interactions.[52,53] Therefore, the influence of the above factors on the adsorption of BPS/BPA by COFs would be discussed in the following.

Firstly, the degree of matching between the pore size of COFs and the molecular dimensions of adsorbates primarily enabled adsorption. Based on the adsorption kinetics and isotherm analysis, both the BPS and BPA molecules were more easily diffused into COF-2 with a larger pore size (25 Å) than COF-1 with a relatively smaller pore size (16 Å). Conversely, there was a relatively low adsorption capacity of BPS and BPA on COF-1. Furthermore, BPS exhibited higher adsorption capacities than BPA, which may have been related to the different molecular structures and properties of these two chemicals. The –SO$_2$– group presented in BPS may play a critical role in promoting the adsorption of BPS on COFs. On the one hand, BPS contained a strong electron-withdrawing sulfonyl group, which could enhance the π–π interaction between BPS and benzene ring on COFs.[54] On the other hand, compared to BPA, the electron-withdrawing sulfonyl group could also enhance the acidic of BPS, which further promoted the Lewis acid–base interaction

between BPS and COFs. Because the existence of lone pair electrons on the nitrogen-containing functional group(–C=N–), COFs could act as Lewis base for binding acidic bisphenol molecules through Lewis acid–base interaction. These results indicated that π–π interaction and Lewis acid–base interaction played significant roles in the adsorption process.[55]

Secondly, given that the hydrophobic benzene ring skeleton of the COFs and hydrophobic properties of BPS and BPA pollutants, according to the "like dissolves like" principle, the hydrophobic molecules tended to enter into the COFs.[56] Thus, the adsorption capacity of COFs materials for bisphenols likely enhanced with the increase of hydrophobicity. However, in this study, the COFs demonstrated an improved adsorption capacity for BPS, although the hydrophobicity of BPS ($\log K_{ow} = 1.65$) was lower than that of BPA ($\log K_{ow} = 3.32$).[57] This signified that the hydrophobic interaction was not the dominant mechanism for the adsorption of BPS/BPA on COFs, and there were likely several other mechanisms that prominently governed the adsorption process. In addition, based on the analysis of the pH effects, the electrostatic attraction would not occur between the COFs and bisphenols within the pH 4–7 range, indicating that electrostatic interaction could not justify the adsorption process. However, electrostatic repulsion may likely have a significant inhibitory role in other interactions, such as hydrogen bonding and π–π interactions, resulting in a reduced adsorption capacity in the pH values range of 8–11.[58]

Thirdly, hydrogen bonds were likely to be a predominant factor that controlled the adsorption of BPS/BPA onto COFs due to both molecules possessing abundant hydrogen donors and acceptors.[59] To verify this mechanism, high-resolution N 1s were recorded. As shown in Fig. 6(a and b), the N 1s peak of COFs shifted to low energy after being loaded BPA and BPS. Subsequent to BPA loading of COF-1 and COF-2, the C=N shifted from 399.5 eV and 399.4 eV to 398.9 eV and 399.3 eV, respectively. Following the BPS loading of COF-1 and COF-2, the C=N also shifted from 399.5 eV and 399.4 eV to 399 eV and 398.9 eV, respectively. These results indicated that hydrogen bonds were likely generated between –OH and C=N groups.

Furthermore, π–π interactions were also believed to be the mainly mechanism for the increased adsorption of aromatic chemicals onto the COFs.[60] On the one hand, the surfaces of the COFs contained abundant conjugated π domains as π acceptors.[61] Conversely, as an electron-donating group, –OH made the benzene rings of BPS/BPA electron-rich.[62] Thus, we expected that BPS/BPA could be adsorbed on COFs via π–π interactions between the benzene rings of the COFs and BPA. To demonstrate this adsorption mechanism, changes in the XPS spectra prior to and following the adsorption of BPA onto COF-1 and COF-2 were recorded. As shown in Fig. 6(c and d), once BPA was loaded to COF-1, the C 1s deconvolutions of C=C, C–C, and C=N shifted from 284.5 eV, 286 eV and 288.9 eV to 284.4 eV, 285.4 eV, and 288.7 eV, respectively. Similar results could be also observed for BPA loaded COF-2, where the C=C, C–C and C=N shifted from 284.4 eV, 285.9 eV, and 288.9 eV to 284.3 eV, 285.3 eV and 288.8 eV. The high π electron density of BPA loaded on COF leaded to lower photon resonance energy values
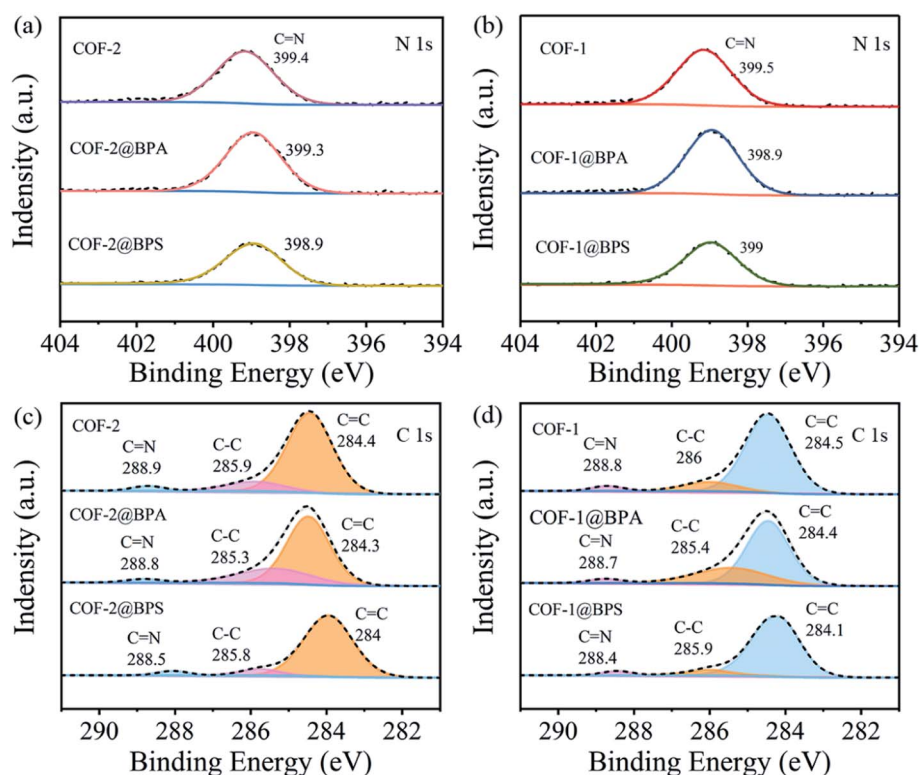
Fig. 6 (a and b) High deconvolutions of N 1s spectra of before and after adsorption of BPS and BPA onto COF-1 and COF-2; (c and d) high deconvolutions of C1s spectra of before and after adsorption of BPS and BPA onto COF-1 and COF-2.

to excite aromatic carbons.[63] For BPS, after loaded on COF-1, the C 1s deconvolutions of C=C, C–C, and C=N shifted from 284.5 eV, 286 eV and 288.8 eV to 284.1 eV, 285.9 eV, and 288.4 eV, respectively. And after loaded on COF-2, the C 1s deconvolutions of C=C, C–C, and C=N also shifted from 284.4 eV, 285.9 eV, and 288.9 eV to 284 eV, 285.8 eV and 288.5 eV. Additionally, the S 2p high-resolution spectrum (Fig. S4†) indicated the successful adsorption of BPS on COFs.

Moreover, the FT-IR spectra of COF-1 and COF-2 prior to and following adsorption were also recorded to further interpret this mechanism. As shown in Fig. 7(a), compared with the COFs before adsorption, a wide band of –OH extending at 3430 cm^{-1} was observed on the spectra of COF-1 and COF-2 after adsorbing BPS/BPA. This indicated that –OH likely played a key role in the adsorption process. Several reports confirmed that –OH played an important role in the form of hydrogen bonds between materials and pollutants, which was conducive for the adsorption of organic pollutants.[64,65] Moreover, the absorption band corresponding to the aromatic –C=N– stretching vibration in the COFs spectrum was strengthened following the adsorption of BPS/BPA. An obvious enhancement was observed for the peaks at 1510 cm^{-1} and 827 cm^{-1}, which was ascribed to the stretching vibration of C–H and the bending vibration of the aromatic rings, which finally verified the adsorption of BPS and BPA on the COFs.[58] In particular, COF-2 exhibited a stronger peak at 1510 cm^{-1} and 827 cm^{-1} following adsorption in contrast to COF-1, which indicated that COF-2 had more potent π–π interactions.

Additionally, the different types of pharmaceuticals study further confirmed the adsorption mechanism (Fig. 3). COF-2

had a stronger adsorption performance for the three selected types of pollutants than did COF-1, suggesting that COF-2 with a larger pore size was more favorable for the diffusion and adsorption of pollutants. The adsorption capacities of the as-prepared COFs for these contaminants were ranked as follows: bisphenols pharmaceuticals > anti-inflammatory pharmaceuticals > sulfa pharmaceuticals.

Compared with bisphenols, the adsorption capacity of the COFs was obviously decreased for anti-inflammatory pharmaceuticals and sulfa pharmaceuticals with fewer hydroxyl groups. This indicated interactive hydrogen bonding between the hydroxyl groups of the bisphenols and –C=N– groups of the COFs, as well as the importance of the molecular dimensions of pollutants in adsorption. Conversely, the relatively high adsorption capacities for bisphenols were arranged as follows: BPB > BPS > BPAF > BPA > BPF. This may have been related to the molecular dimensions of the bisphenols. Table 1 showed that except BPB, with the larger molecular sizes of bisphenols, their diffusion into the COF channels was reduced, which resulted in a decreased-adsorption capacity. In addition, the COFs showed a higher adsorption capacity for BPB than the other bisphenols, although its molecular size was not the smallest. This may have been attributed to hydrophobic influences, hydrogen bonding, and π–π interactions.

3.5. Regeneration experience

Aside from excellent adsorption performance, the regeneration and reusability of adsorbents are essential for practical applications. COF-2 was selected as a reference for the reusability. To
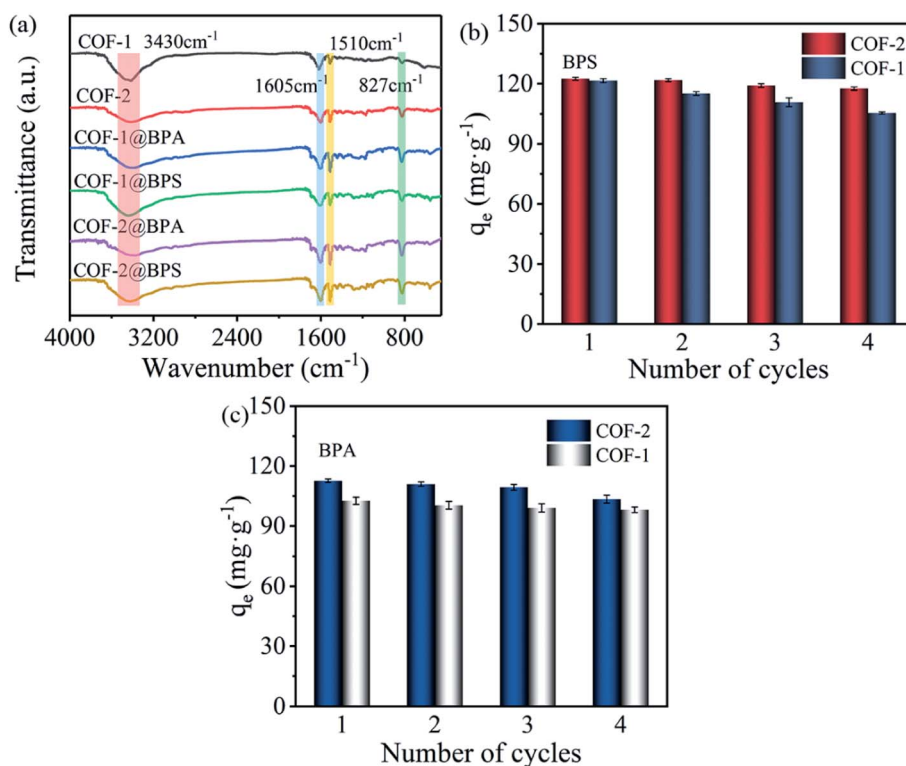
Fig. 7 (a) FT-IR spectra of before and after adsorption of BPS and BPA onto COF-1 and COF-2; (b and c) regeneration test of COF-1 and COF-2 for the adsorption of BPS and BPA (adsorption: $C_0 = 30$ mg L^{-1}, $T = 303$ K, $t = 3$ h, $m/V = 0.2$ g L^{-1}; desorption with methanol, $t = 1$ h, $V = 40$ ml).

17 P. Pachfule, A. Acharjya, J. Roeser, T. Langenhahn, M. Schwarze, R. Schomäcker, A. Thomas and J. Schmidt, *J. Am. Chem. Soc.*, 2018, **140**, 1423–1427.

18 Y. Xu, X. Shi, R. Hua, R. Zhang, Y. Yao, B. Zhao, T. Liu, J. Zheng and G. Lu, *Appl. Catal., B*, 2020, **260**, 118142.

19 S. Chandra, T. Kundu, K. Dey, M. Addicoat, T. Heine and R. Banerjee, *Chem. Mater.*, 2016, **28**, 1489–1494.

20 Y. Li, C. Wang, S. Ma, H. Zhang, J. Ou, Y. Wei and M. Ye, *ACS Appl. Mater. Interfaces*, 2019, **11**, 11706–11714.

21 Y. Shen, C. Zhu, S. Song, T. Zeng, L. Li and Z. Cai, *Environ. Sci. Technol.*, 2019, **53**, 9091–9101.

22 S. Zhuang, R. Chen, Y. Liu and J. Wang, *J. Hazard. Mater.*, 2020, **385**, 121596.

23 Z. Liu, H. Wang, J. Ou, L. Chen and M. Ye, *J. Hazard. Mater.*, 2018, **355**, 145–153.

24 Y. Jiang, C. Liu and A. Huang, *ACS Appl. Mater. Interfaces*, 2019, **11**, 32186–32191.

25 G. Li, J. Ye, Q. Fang and F. Liu, *Chem. Eng. J.*, 2019, **370**, 822–830.

26 X. Liu, H. Xu, L. Wang, Z. Qu and N. Yan, *Chem. Eng. J.*, 2020, **381**, 122559.

27 H. Wang, T. Wang, R. Ma, K. Wu, H. Li, B. Feng, C. Li and Y. Shen, *J. Taiwan Inst. Chem. Eng.*, 2020, **112**, 122–129.

28 F. Pan, W. Guo, Y. Su, N. A. Khan, H. Yang and Z. Jiang, *Sep. Purif. Technol.*, 2019, **215**, 582–589.

29 S.-X. Xu, Z.-Q. Yao and Y.-H. Zhang, *Eur. Polym. J.*, 2020, **133**, 109764.

30 C. Yuan, X. Wu, R. Gao, X. Han, Y. Liu, Y. Long and Y. Cui, *J. Am. Chem. Soc.*, 2019, **141**, 20187–20197.

31 W. Ma, Q. Zheng, Y. He, G. Li, W. Guo, Z. Lin and L. Zhang, *J. Am. Chem. Soc.*, 2019, **141**, 18271–18277.

32 B. J. Smith, A. C. Overholts, N. Hwang and W. R. Dichtel, *Chem. Commun.*, 2016, **52**, 3690–3693.

33 Y. Pramudya and J. L. Mendoza-Cortes, *J. Am. Chem. Soc.*, 2016, **138**, 15204–15213.

34 A. Nagai, Z. Guo, X. Feng, S. Jin, X. Chen, X. Ding and D. Jiang, *Nat. Commun.*, 2011, **2**, 536.

35 Y. Pramudya and J. L. Mendoza-Cortes, *J. Am. Chem. Soc.*, 2016, **138**, 15204–15213.

36 C. Yuan, X. Wu, R. Gao, X. Han, Y. Liu, Y. Long and Y. Cui, *J. Am. Chem. Soc.*, 2019, **141**, 20187–20197.

37 L. Bai, S. Z. F. Phua, W. Q. Lim, A. Jana, Z. Luo, H. P. Tham, L. Zhao, Q. Gao and Y. Zhao, *Chem. Commun.*, 2016, **52**, 4128–4131.

38 L. Su, Y. Xiong, H. Yang, P. Zhang and F. Ye, *J. Mater. Chem. B*, 2016, **4**, 128–134.

39 X. Li, Q. Gao, J. Wang, Y. Chen, Z.-H. Chen, H.-S. Xu, W. Tang, K. Leng, G.-H. Ning, J. Wu, Q.-H. Xu, S. Y. Quek, Y. Lu and K. P. Loh, *Nat. Commun.*, 2018, **9**, 2335.

40 X. Wang, X. Han, J. Zhang, X. Wu, Y. Liu and Y. Cui, *J. Am. Chem. Soc.*, 2016, **138**, 12332–12335.

41 W. Sun, H. Li, H. Li, S. Li and X. Cao, *Chem. Eng. J.*, 2019, **360**, 645–653.

42 Y. Li, C.-X. Yang and X.-P. Yan, *Chem. Commun.*, 2017, **53**, 2511–2514.

43 M. Monier and D. A. Abdel-Latif, *J. Hazard. Mater.*, 2012, **209–210**, 240–249.

44 P. Wu, Z. Cai, H. Jin and Y. Tang, *Sci. Total Environ.*, 2019, **650**, 671–678.

45 Y. Zhang, Y. Cheng, N. Chen, Y. Zhou, B. Li, W. Gu, X. Shi and Y. Xian, *J. Colloid Interface Sci.*, 2014, **421**, 85–92.

46 L. Wang, A. Li and Y. Chang, *Chem. Eng. J.*, 2016, **297**, 1–10.

47 F. F. Liu, J. Zhao, S. Wang, P. Du and B. Xing, *Environ. Sci. Technol.*, 2014, **48**, 13197–13206.

48 S. Zhang, T. Shao, S. S. K. Bekaroglu and T. Karanfil, *Water Res.*, 2010, **44**, 2067–2074.

49 M. A. Fontecha-Cámara, M. V. López-Ramón, M. A. Álvarez-Merino and C. Moreno-Castilla, *Langmuir*, 2007, **23**, 1242–1247.

50 U. Suntisukaseam, P. Weschayanwuwat and D. A. Sabatini, *Environ. Eng. Sci.*, 2007, **24**, 1457.

51 Z. Hasan, N. A. Khan and S. H. Jhung, *Chem. Eng. J.*, 2016, **284**, 1406–1413.

52 Z. Hasan and S. H. Jhung, *J. Hazard. Mater.*, 2015, **283**, 329–339.

53 W. Wang, S. Deng, L. Ren, D. Li, W. Wang, M. Vakili, B. Wang, J. Huang, Y. Wang and G. Yu, *ACS Appl. Mater. Interfaces*, 2018, **10**, 30265–30272.

54 H. Guo, H. Li, N. Liang, F. Chen, S. Liao, D. Zhang, M. Wu and B. Pan, *Environ. Sci. Pollut. Res.*, 2016, **23**, 8976–8984.

55 G. Li, X. Zhang, J. Sun, A. Zhang and C. Liao, *J. Hazard. Mater.*, 2020, **381**, 120985.

56 L. Xie, D. Yang, Q. Lu, H. Zhang and H. Zeng, *Curr. Opin. Colloid Interface Sci.*, 2020, **47**, 58–69.

57 L.-H. Wu, X.-M. Zhang, F. Wang, C.-J. Gao, D. Chen, J. R. Palumbo, Y. Guo and E. Y. Zeng, *Sci. Total Environ.*, 2018, **615**, 87–98.

58 Y. Lv, J. Ma, K. Liu, Y. Jiang, G. Yang, Y. Liu, C. Lin, X. Ye, Y. Shi, M. Liu and L. Chen, *J. Hazard. Mater.*, 2021, **403**, 123666.

59 Z. Sun, L. Zhao, C. Liu, Y. Zhen and J. Ma, *Chem. Eng. J.*, 2020, **381**, 122510.

60 S. Yu, X. Wang, W. Yao, J. Wang, Y. Ji, Y. Ai, A. Alsaedi, T. Hayat and X. Wang, *Environ. Sci. Technol.*, 2017, **51**, 3278–3286.

61 W. Wang, S. Deng, L. Ren, D. Li, W. Wang, M. Vakili, B. Wang, J. Huang, Y. Wang and G. Yu, *ACS Appl. Mater. Interfaces*, 2018, **10**, 30265–30272.

62 W. Chen, L. Duan, L. Wang and D. Zhu, *Environ. Sci. Technol.*, 2008, **42**, 6862–6868.

63 A. Kuznetsova, I. Popova, J. T. Yates, M. J. Bronikowski, C. B. Huffman, J. Liu, R. E. Smalley, H. H. Hwu and J. G. Chen, *J. Am. Chem. Soc.*, 2001, **123**, 10699–10704.

64 K. Liu, Z. Huang, J. Dai, Y. Jiang, G. Yang, Y. Liu, C. Lin, Y. Lv and M. Liu, *Chem. Eng. J.*, 2020, **382**, 122775.

65 Y. Lv, R. Zhang, S. Zeng, K. Liu, S. Huang, Y. Liu, P. Xu, C. Lin, Y. Cheng and M. Liu, *Chem. Eng. J.*, 2018, **339**, 359–368.